Bioconjugate Chemistry

Article

pubs.acs.org/bc

Cys34-PEGylated Human Serum Albumin for Drug Binding and Delivery

Jonathan G. Mehtala,[†] Chris Kulczar,[‡] Monika Lavan,[‡] Gregory Knipp,*[,‡] and Alexander Wei*[,†]

[†]Department of Chemistry [‡]Department of Industrial and Physical Pharmacy, Purdue University, West Lafayette, Indiana 47907, United States

Supporting Information

ABSTRACT: Polyethylene glycol (PEG) derivatives were conjugated onto the Cys-34 residue of human serum albumin (HSA) to determine their effects on the solubilization, permeation, and cytotoxic activity of hydrophobic drugs such as paclitaxel (PTX). PEG(C34)HSA conjugates were prepared on a multigram scale by treating native HSA (n-HSA) with 5- or 20-kDa mPEG-maleimide, resulting in up to 77% conversion of the mono-PEGylated adduct. Nanoparticle tracking analysis of PEG(C34)HSA formulations in phosphate buffer revealed an increase in the number of nanosized aggregates relative to n-HSA, both in the absence and presence of PTX. Cell viability studies conducted with MCF-7 breast cancer cells indicated that PTX cytotoxicity was enhanced by PEG(C34)HSA when mixed at 10:1 mol ratios, up to a 2-fold increase in potency relative to n-HSA. The PEG(C34)HSA conjugates were also evaluated as PTX carriers across monolayers of HUVEC and hCMEC/D3 cells, and found to have permeation profiles nearly identical to those of n-HSA.

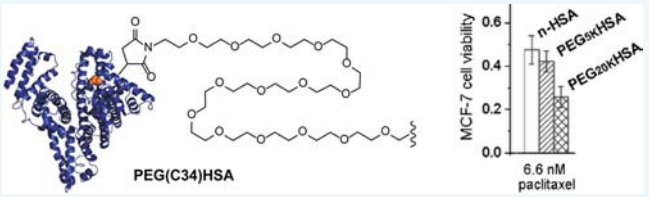

INTRODUCTION

Protein function and recognition can be rationally modified by the covalent ligation of molecular structures such as optical tags,[1] targeting ligands,[2] carbohydrates,[3] and polymers.[4,5] However, coupling methods that rely on available amines or carboxylic acids for amide bond formation typically have poor regioselectivity and can result in intra- or intermolecular cross-links that lead to protein denaturation, aggregation, or general loss of function.[6] Site-specific ligation methods are highly desirable for introducing additional functionality to proteins without disrupting other physicochemical properties. A useful alternative to amide bond formation involves the chemoselective addition of alkylmaleimides to exposed cysteines.[7] This method of conjugation has little to no effect on the electrostatic surface potential of proteins at physiological pH and is thus less likely to induce unintended changes in secondary or tertiary structure. *N*- and *C*-modified proteins have the intrinsic drawback of having different net charges relative to the native protein, which can affect their conformational behavior, dispersion stability, aggregation kinetics, biomolecular recognition, and catalytic activity.[6,8,9]

PEGylation (i.e., the ligation of one or more polyethylene glycol chains to external residues) is a widely used tactic to modify the pharmacokinetic properties of drug carriers[10,11] and protein-based biologics.[12,13] Covalently attached PEG chains can stabilize proteins by providing a surrogate hydration shell[14] or prevent denaturation by limiting conformational freedom.[15] While much attention has been paid to antibodies and other "functional" biomolecules, passive proteins such as human serum albumin (HSA) are also important candidates because of their putative roles in drug solubilization and delivery. HSA's native role as a plasma carrier makes it an ideal candidate for transporting hydrophobic drugs that possess higher binding affinities from the bloodstream into extravascular tissue space.[16,17] HSA is thought to facilitate drug permeation by passing through endothelial layers via caveolar-mediated transcytosis.[18,19] As one of most abundant proteins in the plasma (35−50 mg/mL),[20] HSA forms aggregates reversibly and can accumulate passively in tumor tissue due to the enhanced permeability and retention (EPR) effect.[21,22] In this regard, we note that HSA-based formulations have been characterized as nanoparticles *ex vivo* but are thought to disperse into monomeric form soon after entering the bloodstream.[23] This suggests that the pharmacokinetic properties of HSA may be tailored by judicious structural changes.

Interest in albumin-based drug delivery has been increasing due to the favorable pharmacology of HSA, its low immunogenicity, and its current availability in recombinant form. A well-known example of albumin-based formulation is HSA-bound paclitaxel (Abraxane), currently being used for the treatment of several late-stage cancers.[24−26] Paclitaxel (PTX) is a powerful antimitotic that induces apoptosis in rapidly dividing cells;[27] however, its therapeutic efficacy has been compromised by poor water solubility or by surfactants with peripheral side effects (e.g., Cremophore EL).[28−30] The clinical success of Abraxane confirms the benefits of HSA as a carrier of poorly soluble drugs like PTX; nevertheless, adverse side effects such as moderate neuropathy and neutropenia persist,[26,31,32]

Received: March 18, 2015
Revised: April 27, 2015
Published: April 28, 2015

DOI: 10.1021/acs.bioconjchem.5b00143
Bioconjugate Chem. 2015, 26, 941−949

indicating the need to further optimize drug loading and delivery.

PEGylated HSA has been prepared by conventional amide ligation and shown to provide significant enhancements in its pharmacokinetic profile for drug delivery.[33] However, most studies have been conducted by modifying the acidic or basic residues on albumin, and the poor regioselectivity of amide-based ligations render these formulations vulnerable to unintended changes in structure or colligative properties. For example, *N*-PEGylation reduces the volume of the hydrophobic binding cavity in the second R-helix domain, despite overall retention of HSA size and shape.[34]

Both HSA and its congener bovine serum albumin (BSA) possess a free thiol residue at Cys-34, which presents the option of site-specific S-PEGylation using maleimide chemistry.[35,36] S-PEGylation of albumins can be performed with minimal perturbation to pre-existing disulfide bridges with subsequent retention of protein structure, as demonstrated in the case of PEG(C34)BSA,[35] and can increase its circulation lifetime relative to unmodified albumins, as demonstrated in a rat model with PEG(C34)HSA.[36] These reports indicate that S-PEGylation at Cys-34 is an appealing alternative to amide-based ligations for developing albumin-based carriers with tailored pharmacological properties. It is worth mentioning that maleimide-based reagents have also been developed for PEGylation across disulfide bonds[37,38] but are not immediately relevant for proteins bearing free thiols.

In this article, we characterize the carrier properties of two mono-PEGylated HSA derivatives with site-specific conjugation at Cys-34, prepared on a multigram scale using maleimide-terminated mPEG chains having molecular weights of 5 and 20 kDa. S-PEGylation produces minimal perturbations in conformation or solubilization of PTX but significantly increases HSA's propensity to self-assemble into protein nanoparticles as characterized by nanoparticle tracking analysis (NTA). We also investigate the permeation of PTX through monolayers of human umbilical vascular endothelial cells (HUVEC) and brain microvascular endothelial cells (hCMEC/D3) with and without PEG(C34)HSA conjugates, and evaluate the therapeutic efficacy of PTX-loaded PEG(C34)HSA against MCF-7 breast cancer cells relative to native HSA (n-HSA). We find that C34-PEGylation has essentially no negative impact on PTX loading and subsequent permeation across cell monolayers. However, PEG(C34)HSA conjugates provide substantial increases in the transport and cytotoxicity of PTX delivered to MCF-7 cells, with negligible toxicity from PEGylated HSA alone.

RESULTS AND DISCUSSION

Synthesis and Characterization of PEGylated HSA Adducts. Following an earlier reported procedure,[36] PEG-(C34)HSA adducts were prepared at 37 °C in mildly acidic PBS (pH 6.5) by combining n-HSA (25 mg/mL) with 2 or 4 equivs of 5-kDa or 20-kDa mPEG-Mal (Scheme 1). Maintaining a pH slightly below 7 helps to keep HSA in conformations that shield its internal disulfide bonds from other solutes.[39] Analytical samples of S-PEGylated HSA were obtained by HPLC purification, whereas protein mixtures synthesized on a multigram scale were separated from unreacted mPEG-Mal by stirred ultrafiltration. Recombinant HSA was used instead of plasma-derived HSA, which reduces the risk of infection from unknown viruses or prions that may be present in the latter. Recombinant and plasma-derived HSA have been shown to be identical in structure.[40]

Scheme 1. Synthesis of PEG(C34)HSA Using 5- or 20-kDa mPEG-Maleimide (Mal)[a]

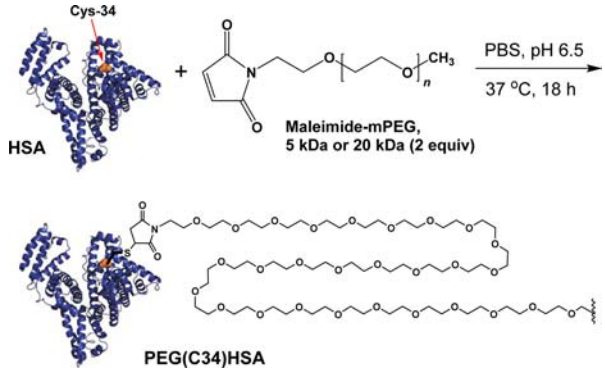

[a]The PEG chain is truncated for clarity.

MALDI-MS and analytical HPLC were used to assess the degree of PEGylation: n-HSA produced a strong peak at m/z 66,553,[41] whereas PEG_{5K}- and PEG_{20K}(C34)HSA produced additional peak sets centered at 71,984 (+5,431 amu) and 87,694 (+21,141 amu), respectively (Figure 1a–c). HPLC analysis on dialyzed samples indicated that treatment of n-HSA (*Rt* 6.4 min) with two equivalents of 5-kDa mPEG-Mal supported a 72% conversion into PEG_{5K}(C34)HSA (Figure 1e), whereas treatment with two equivalents of 20-kDa mPEG-Mal supported a 48% conversion into PEG_{20K}(C34)HSA (Figure 1f). The conversion efficiency was not affected by changes in reaction time, temperature, or pH, but increasing the amount of 20-kDa mPEG-Mal to four equivalents increased the conversion of PEG_{20K}(C34)HSA to 77% (Figure S3, Supporting Information). It should be noted that the HSA was not pretreated with reducing agents, which can further optimize maleimide addition to free cysteines;[42] therefore, the yields reported here should be viewed as a lower limit. We also note that ultrafiltration of PEG(C34)HSA from excess mPEG-Mal on a multigram scale was initially tedious due to the high viscosity of the retentate but became more efficient after several washings, with less than 1 wt % mPEG after six cycles according to HPLC (Figure S4, Supporting Information). All subsequent studies using PEG(C34)HSA were performed with protein mixtures prepared from a 2:1 ratio of mPEG-Mal to n-HSA, and purified by six cycles of ultrafiltration.

ATR-IR analysis confirmed the retention of the PEG chain after exhaustive dialysis, with a strong peak at 1090 cm^{-1} corresponding to C–O stretching modes, and minimal differences in the amide peak region relative to n-HSA (Figure S2, Supporting Information). Circular dichroism analysis of the PEG-(C34)HSA derivatives also indicated negligible changes in secondary protein structure relative to n-HSA, with very minor perturbations in the 195–260 nm region (Figure 2). We thus presume that S-PEGylation at Cys-34 has minimal influence on the secondary structure of HSA.

Effect of PTX-HSA Formulations on Cell Viability. MCF-7 cells exposed to 10 nM PTX using a 30:1 mol ratio of PTX/n-HSA had a 1.7-fold greater therapeutic effect compared to that of 10 nM PTX in PBS without HSA ($p < 0.05$), whereas PTX formulated in a 10:1 mol ratio with n-HSA had 3.1-fold greater efficacy ($p < 0.005$; Figure 3).[43] HSA without PTX (up to 100 nM) had a negligible effect on cell viability, confirming that its primary role is to increase the solubilization of PTX. The increased drug efficacy did not vary significantly for PTX/

DOI: 10.1021/acs.bioconjchem.5b00143
Bioconjugate Chem. 2015, 26, 941–949

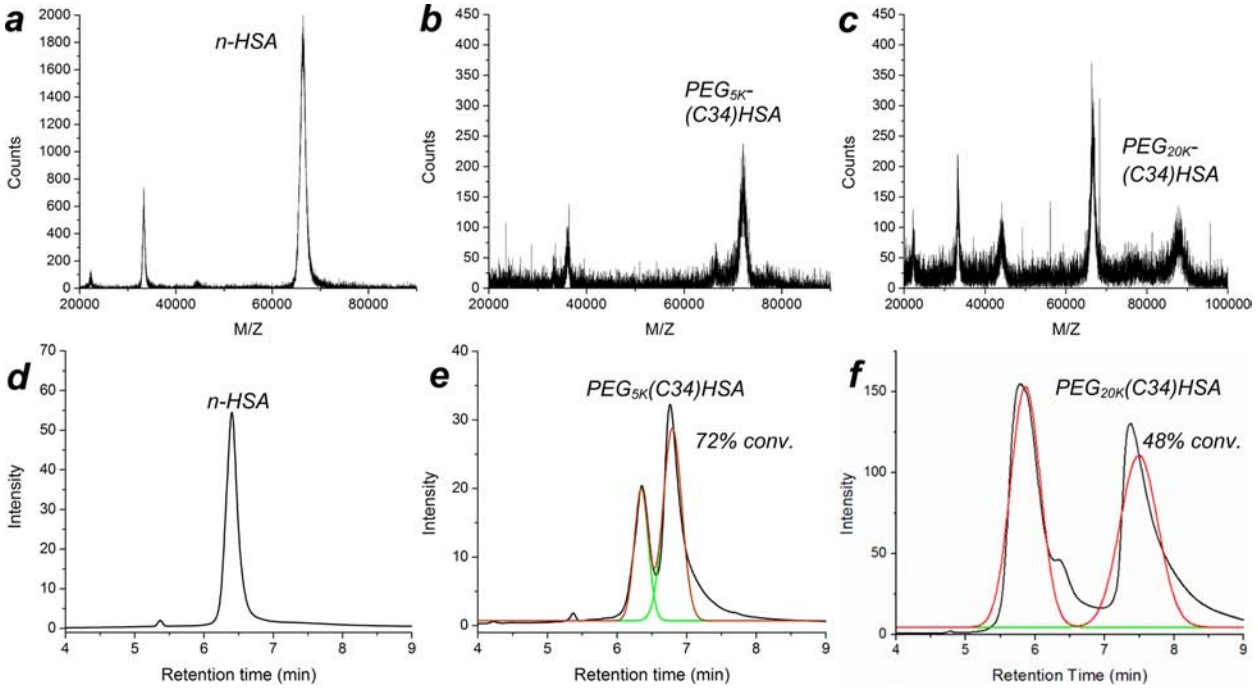

Figure 1. (a–c) MALDI-MS analysis of n-HSA (m/z ~66.5 kDa), PEG_{5K}(C34)HSA (m/z ~72.0 kDa), and PEG_{20K}(C34)HSA (m/z ~87.7 kDa); (d–f) HPLC traces of n-HSA (as received), HSA treated with 2 equiv of $mPEG_{5K}$-Mal or 2 equiv of $mPEG_{20K}$-Mal. For additional data, see Figures S3 and S4, and Table S1 (Supporting Information).

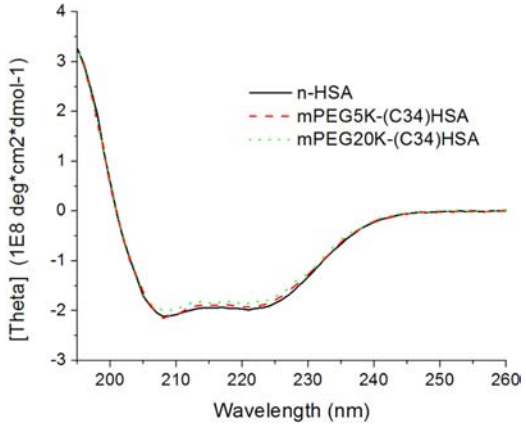

Figure 2. Circular dichroism spectra of n-HSA, PEG_{5K}(C34)HSA (72% conversion), and PEG_{20K}(C34)HSA (77% conversion).

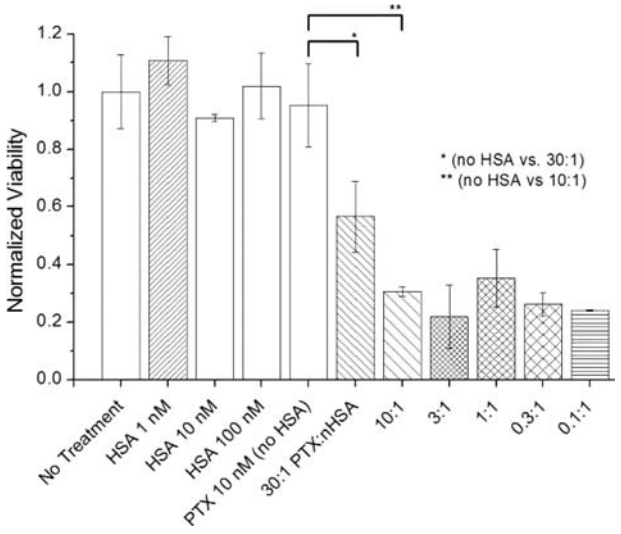

Figure 3. Effect of formulating PTX (10 nM) with n-HSA on MCF-7 cell cultures, 5 days post-treatment (N = 3). PTX/n-HSA mole ratios range from 30 to 0.1, with [PTX] fixed at 10 nM. Significant changes in cytotoxicity marked with * (p < 0.05) or ** (p < 0.005). Error = 1 stdev.

n-HSA ratios below 10:1, implying an upper limit of 10 molecules of PTX per HSA carrier.

MCF-7 cells exposed to 10 nM PTX in a 10:1 mol ratio of PTX and PEG_{5K}(C34)HSA or PEG_{20K}(C34)HSA experienced similar increases in toxicity relative to that of PTX alone (Figure 4). As in the case with n-HSA, maximum efficacy was attained when PTX was formulated in a 10:1 mol ratio with PEG(C34)HSA derivatives compared to a 30:1 ratio, with no further improvements below that. These results imply that the PEG chain does not inhibit the ability of HSA to bind and release PTX. Again, control experiments indicated that PEGylated HSA derivatives have no effect on cell viability.

MCF-7 cells were exposed to a range of PTX doses (0.3–33 nM) formulated at 10:1 mol ratios with n-HSA, PEG_{5K}(C34)-HSA, or PEG_{20K}(C34)HSA. For intermediate PTX doses (6.6 nM), we observed that formulations with PEG_{20K}(C34)HSA were at least 60% more toxic than that of PEG_{5K}(C34)HSA (p < 0.05) and 80% more toxic than that of n-HSA (p < 0.01; Figure 5). A linear interpolation of cytotoxicity data at 3.3 and 6.6 nM yields IC_{50} values of 6.5, 5.9, and 4.7 nM when PTX is formulated, respectively, with 10 mol% of n-HSA, PEG_{5K}(C34)HSA, and PEG_{20K}(C34)HSA, with the latter providing a nearly 40% increase in acute cytotoxicity relative to n-HSA. While the basis for the greater potency provided by PEG_{20K}(C34)HSA has not yet been elucidated, we observe an intriguing correlation with changes in the self-association behavior of HSA induced by Cys-34 tethered mPEG chains (see below).

DOI: 10.1021/acs.bioconjchem.5b00143
Bioconjugate Chem. 2015, 26, 941–949

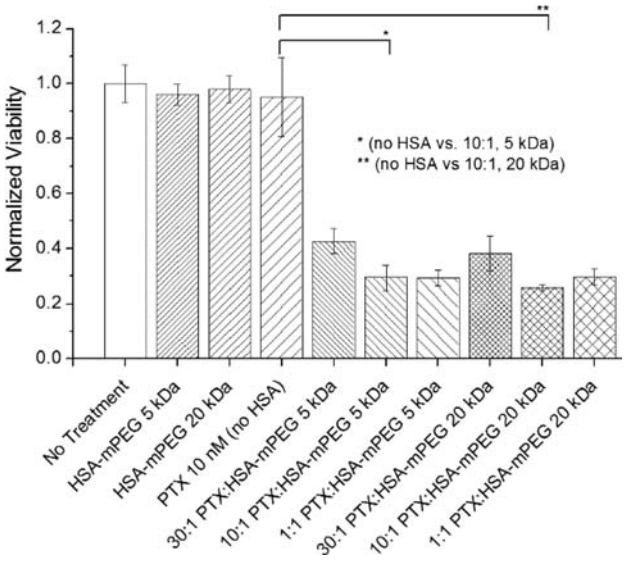

Figure 4. Effects of PTX (10 nM) formulated with PEG_{5K}(C34)HSA or PEG_{20K}(C34)HSA on MCF-7 cell cultures, 5 days post-treatment, with [PTX] fixed at 10 nM (PTX/HSA = 30−0.1; $N = 3$). Significant changes in cytotoxicity are marked with * and ** ($p < 0.005$). Error = 1 stdev.

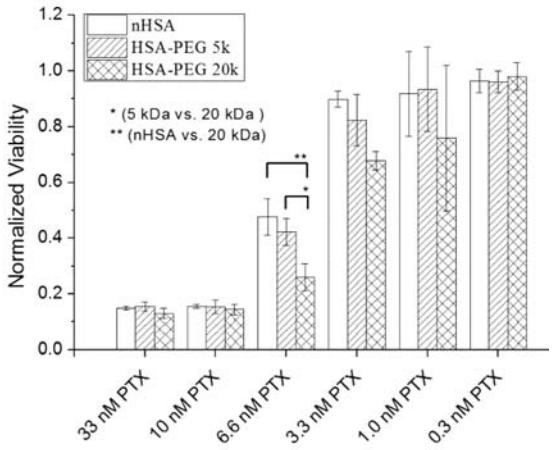

Figure 5. Cytotoxicity of PTX (0.3−33 nM) formulated in a 10:1 mol ratio with n-HSA, PEG_{5K}(C34)HSA, or PEG_{20K}(C34)HSA (MCF-7 cells, 5 days post-treatment; $N = 3$). Significant changes in cytotoxicity marked with * ($p < 0.05$) or ** ($p < 0.01$). Error = 1 stdev.

Effects of PEGylation and PTX on Protein Nanoparticle Formation. Nanoparticle tracking analysis (NTA) was used to measure the hydrodynamic size (d_h) and concentration of submicron protein aggregates in PBS (pH 6.5). In nearly all cases, multimodal distributions were obtained with a wide variance (range of 100−400 nm); however, a comparison between data sets revealed clear differences in population sizes. At high protein concentration (1 mg/mL or 13−15 μM), mixtures containing PEG_{5K}- and PEG_{20K}(C34)-HSA formed several times more nanoparticles than n-HSA (Figure 6a), while their d_h and volumetric mean values (d_{vol}) remained roughly the same (Table 1). At 10-fold lower concentration (0.1 mg/mL or 1.3−1.5 μM), suspensions with PEGylated HSA again showed a higher number of nanoaggregates relative to pure n-HSA (Figure 6b). Although these concentrations are substantially higher than those used in the

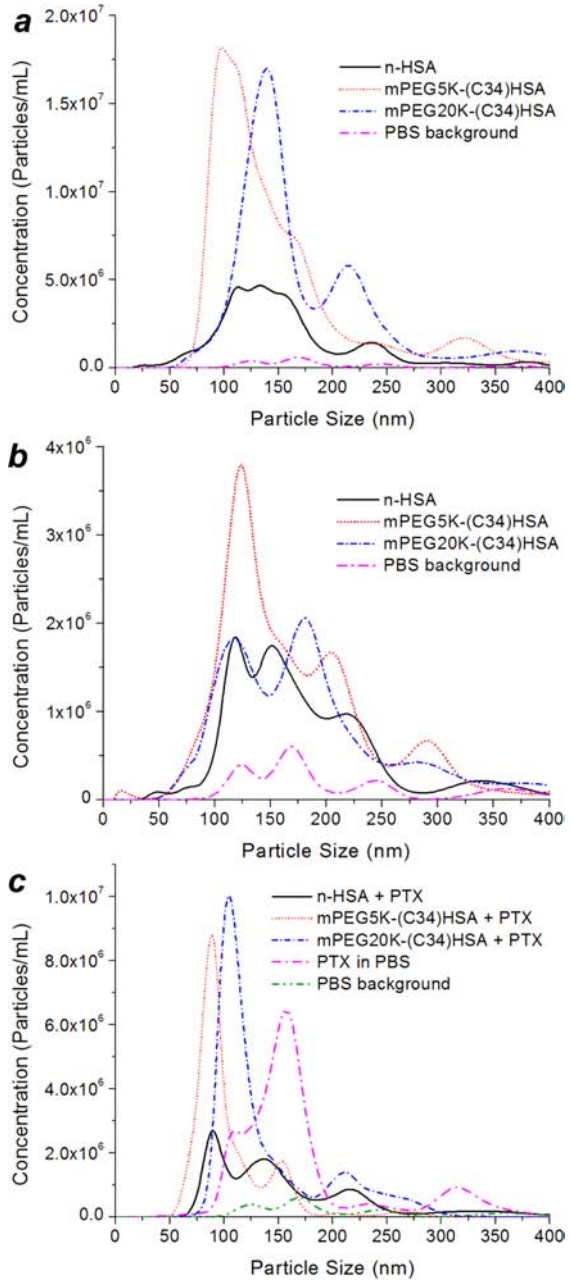

Figure 6. Hydrodynamic size analysis and number distribution of HSA nanoparticles by NTA, for mixtures comprising n-HSA, PEG_{5K}(C34)-HSA, and PEG_{20K}(C34)HSA in PBS. (a) 1 mg/mL (13−15 μM), (b) 0.1 mg/mL (1.3−1.5 μM), and (c) 0.1 mg/mL with 10 equiv of PTX. A plot of PTX aggregates in PBS without HSA ([PTX] = 12.5 μM) is included for comparison.[44]

cytotoxicity assays, they show that S-PEGylation promotes HSA nanoparticle formation. It is worth noting that dynamic light scattering analysis of pure PEG_{20K}(C34)HSA at 0.01 mg/mL also indicates nanoparticle formation (d_h = 30−80 nm), whereas n-HSA at the same concentration is essentially monomeric.[36]

The effects of PEGylation on the spontaneous formation of HSA nanoparticles were also evident for excipients formulated with PTX at a 10:1 mol ratio. At low carrier concentration (0.1 mg/mL), mixtures with PEG_{5K}- and PEG_{20K}(C34)HSA formed aggregates with a narrower, bimodal distribution relative to n-HSA (Figure 6c).[44] It is worth noting that the number of n-

DOI: 10.1021/acs.bioconjchem.5b00143
Bioconjugate Chem. 2015, 26, 941−949

Table 1. Statistical Analysis of HSA Nanoparticles by NTA

sample	particle count ($\times 10^6$ mL^{-1})[a]	mode peaks[b]	hydrodynamic size (nm)			
			mean (d_h)	RSD (%)	d_{vol}[c]	RSD (%)
		1 mg/mL (No PTX)				
n-HSA	258	100–160 (broad), 235	162	48	200	43
mPEG$_{5K}$(C34)HSA	745	100, 320	152	51	195	45
mPEG$_{20K}$(C34)HSA	671	140, 220	188	50	237	45
		0.1 mg/mL (No PTX)				
n-HSA	92	120, 150, 225, 340	192	37	219	35
mPEG$_{5K}$(C34)HSA	221	125, 210, 290	166	48	206	43
mPEG$_{20K}$(C34)HSA	157	120, 180, 290	182	48	227	44
		0.1 mg/mL (10:1 PTX/HSA)				
n-HSA	123	90, 140, 220	189	65	264	54
mPEG$_{5K}$(C34)HSA	161	90, 160	105	35	120	33
mPEG$_{20K}$(C34)HSA	225	105, 210	141	43	173	40
PTX, 13 μg/mL[d]	215	110, 160, 310	173	38	198	35

[a]On the basis of the average number of tracks over three runs. [b]>100% above background. [c]Volumetric mean $d_{vol} = (\Sigma n_i d_i^3/N)^{1/3}$, where n_i is the number of particles with size d_i. [d]15 μM PTX with 1% DMSO in PBS; no HSA present.

HSA and PEG$_{20K}$(C34)HSA nanoparticles increased significantly in the presence of PTX, suggesting their formation to be driven partly by the cooperative association of hydrophobic domains. These results reveal the complex interplay between protein concentration, PEG chain length, and the inclusion of PTX on the self-assembly of HSA nanoparticles in physiologically relevant conditions.

Effect of Formulations on PTX Permeability. Monolayers of HUVEC and hCMEC/D3 cells were initially tested to examine the effect of n-HSA and mPEG(C34)HSA on PTX permeability, using a [^{14}C]-labeled drug. HUVEC monolayers are used to model the peripheral vasculature, whereas the hCMEC/D3 monolayers are representative of the blood–brain barrier.[45,46] Studies were run at 1 μM [^{14}C]-PTX alone and in 10:1 mol ratio with n-HSA or mPEG(C34)HSA, preceded by a 4-h pre-equilibration period for the cell monolayers (Figure 7).[47] The HSA formulations did not produce significant differences in [^{14}C]-PTX permeation across either cell monolayer, which suggests that the binding and permeation of free PTX may be reversible. However, HUVEC monolayers exhibited significantly faster permeability rates, implying that PTX permeates more readily into the vascular periphery relative to the brain. This is expected, as hCMEC/D3 cells express high levels of efflux transporters such as P-glycoprotein that are active against PTX.[48]

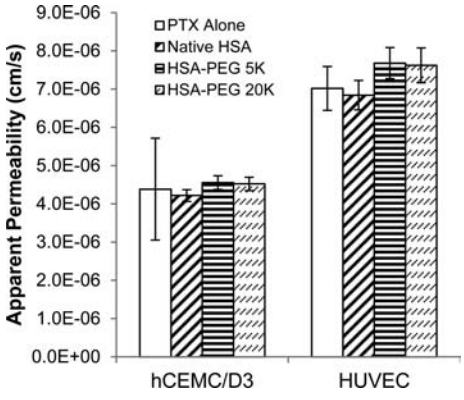

Figure 7. Permeability of 1 μM [^{14}C]-paclitaxel across hCMEC/D3 and HUVEC monolayers. Studies were run in triplicate simultaneously using a 10:1 mol ratio of PTX/n-HSA or PEG(C34)HSA (error = 1 stdev).

The effect of PTX concentration on HSA-mediated permeability was also investigated. P_{app} values across HUVEC monolayers were initially obtained at 0.5, 1, 10, and 25 μM PTX in a 10:1 mol ratio with n-HSA or PEG(C34)HSA, following pre-equilibration. Studies conducted at 0.5 and 1 μM PTX contained only the [^{14}C]-labeled drug, whereas higher concentrations were made from an unlabeled drug supplemented with 1 μM [^{14}C]PTX. At low solute concentrations, n-HSA appears to provide greater permeability then either PEG$_{5K}$(C34)HSA or PEG$_{20K}$(C34)HSA, but at higher concentrations, no significant differences are observed (Figure 8a). The effect of drug–carrier ratio on permeability was also examined at a 5:1 ratio of PTX to n-HSA or PEG(C34)HSA (Figure 8b). In this case, modest decreases in P_{app} values at higher solute concentrations were observed for all three HSA formulations, with minor differences between carrier species.

While P_{app} is useful for delineating possible changes due to partitioning, diffusivity, or variations in free drug for each formulation, it only represents average marker velocities. It is perhaps more important to consider the effects of formulation on drug flux ($P_{app} \times C_0$), which represents the actual amount of drug transferred across the endothelial barrier and is a reliable metric for estimating blood levels. Since flux is concentration-dependent, it better illustrates the effects of solubilizing formulations than the relatively small changes in P_{app}. As expected, large increases in flux are observed for both 10:1 and 5:1 mol ratios of PTX to n-HSA or its S-PEGylated conjugates (Figure 9). Again, S-PEGylation had little to no impact on drug transport, with minor differences attributable to the limited precision typically observed in permeation studies. This establishes that C34-PEGylated HSA can increase PTX efficacy as shown above, without compromising drug solubilization and permeability.

The enhanced efficacy of PTX formulated with PEG$_{5K}$- and especially PEG$_{20K}$(C34)HSA is greatest near its IC$_{50}$ value against MCF-7 breast cancer cells. We also observe that S-PEGylation increases the number of HSA nanoparticles (up to 1.8-fold) relative to n-HSA, particularly in the presence of PTX. While further research is needed to establish the basis for therapeutic enhancement, we consider the following as plausible factors for the observed phenomena: (1) While the

DOI: 10.1021/acs.bioconjchem.5b00143
Bioconjugate Chem. 2015, 26, 941–949

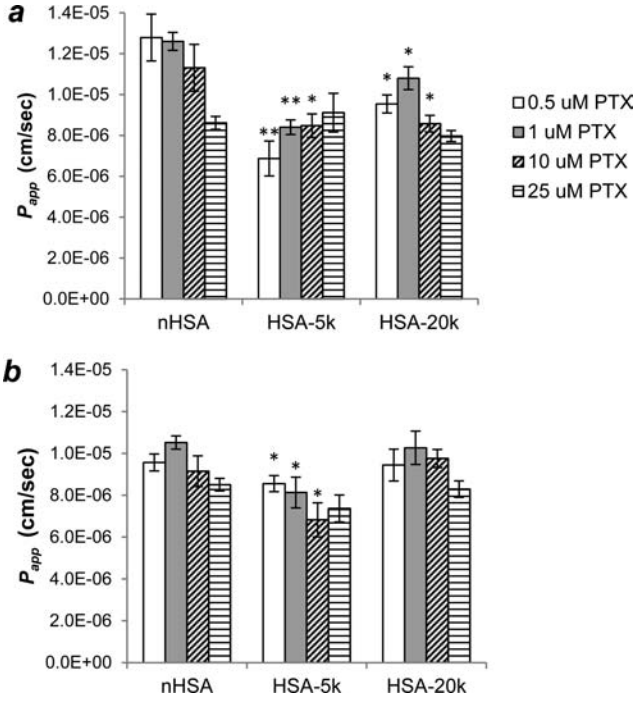

Figure 8. Effect of solute concentration on HSA-mediated HUVEC permeability. (a) P_{app} of [^{14}C]-PTX using a 10:1 mol ratio of PTX to HSA carrier; (b) P_{app} of [^{14}C]-PTX using a 5:1 mol ratio of PTX to HSA carrier. Permeability studies were run in triplicate simultaneously; differences between carriers are marked with * ($p < 0.05$) or ** ($p < 0.01$). Error = 1 stdev.

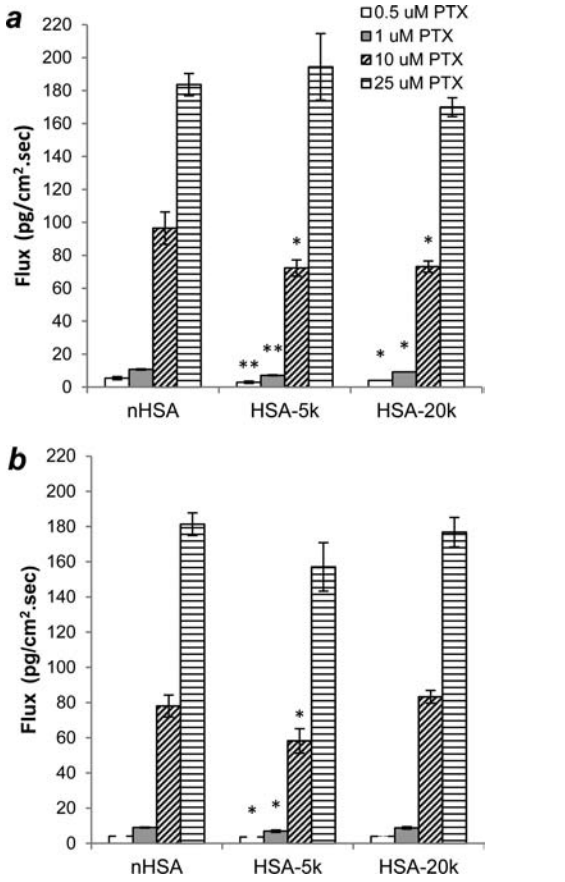

Figure 9. [^{14}C]-PTX flux across HUVEC monolayers using n-HSA or PEG(C34)HSA. (a) 10:1 molar ratio of PTX to HSA carrier; (b) 5:1 molar ratio of PTX to HSA carrier. Permeability studies run in triplicate simultaneously; differences between carriers are marked with * ($p < 0.05$) or ** ($p < 0.01$). Error = 1 stdev.

5- and 20-kDa PEG chains attached to Cys-34 do not disrupt the tertiary structure of HSA, they may reduce its strength of association with bound PTX by increasing its conformational lability; (2) changes in the conformational stability of S-PEGylated HSA may also affect the stability of their aggregates in endosomes, with greater PTX release to the cytoplasm after uptake; and (3) the PEG chains may promote the nano-emulsification of HSA and PTX[49] into forms that are favorably transported by albumin receptors.

In short, while the prescribed benefits of protein PEGylation such as extended stability and circulation times in the bloodstream are well appreciated,[12−15] there appear to be additional factors that may contribute toward favorable pharmacokinetics and drug release profiles and await further validation.

CONCLUSIONS

We have established that the formulation of PTX with PEG_{5K}(C34)HSA and especially PEG_{20K}(C34)HSA enhances its acute toxicity against MCF-7 breast cancer cells relative to native HSA carriers, while retaining high levels of permeability across the monolayers of HUVEC or hCMEC/D3 cells. The latter has important ramifications on the bioavailability of PTX administered by nonintravenous mechanisms, as well as its extravasation into diseased tissue. C34-PEGylation has a notable influence on the size distribution of HSA nanoparticles, which may be partly responsible for the increased cytotoxicity of the PTX payload. Future studies are needed to generalize the therapeutic and pharmacokinetic enhancements of PEG(C34)-HSA-mediated uptake for different classes of hydrophobic drugs, as well as various cancer cell lines and animal tumor models.

MATERIALS AND METHODS

Materials. Recombinant HSA was obtained from GenLantis (San Diego, CA); mPEG-maleimide was obtained from Laysan Bio (Arab, AL); hydrocortisone, Hank's balanced salt solution (HBSS), polystyrene T-75 flasks, and Transwell permeable supports were purchased from Sigma-Aldrich (St. Louis, MO). Paclitaxel was obtained from LC Laboratories (Woburn, MA); and radiolabeled [^{14}C]paclitaxel ([^{14}C]PTX) was purchased from Moravek Biochemicals (Brea, CA). DMEM media, penicillin/streptomycin, and L-glutamine were obtained from Corning Cellgro (Manassas, VA); fetal bovine serum was obtained from Atlanta Biologicals (Atlanta, GA); MTT reagent was obtained from RPI (Mount Prospect, IL); EGM-2, EBM-2, and basic fibroblast growth factor were obtained from Lonza (Walkersville, MD). MCF-7 cells were obtained from the Purdue Center for Combinatorial Chemical Biology; HUVEC cells were obtained from the American Type Culture Collection (ATCC; Manassas, VA); and hCMEC/D3 cells were provided by Dr. Pierre-Olivier Couraud at Institut Cochin (Paris, France). Phosphate buffer solution (PBS) was prepared by 10-fold dilution from a concentrated stock containing 80 g of NaCl, 2 g of KCl, 4 g of Na_2HPO_4, and 2 g of KH_2PO_4. All solutions were prepared using initially deionized water using a Milli-Q ultrafiltration system from Millipore (Bedford, MA) with a measured resistivity above 18 MΩ·cm and passed through a 0.22-μm filter to remove particulate matter.

DOI: 10.1021/acs.bioconjchem.5b00143
Bioconjugate Chem. 2015, 26, 941−949

Gram and Multigram Synthesis of PEG(C34)HSA Conjugates. In a typical reaction, powdered HSA (1.0 g, 15.1 μmol) was dissolved in 40 mL of sterilized PBS (adjusted to pH 6.5) in a 100 mL glass round-bottomed flask. The PBS was passed through a 0.2-μm syringe filter prior to use, and the mixture was stirred for 15 min. $mPEG_{5K}$-Mal (155 mg, 31 μmol) or $mPEG_{20K}$-Mal (620 mg, 31 μmol) was dissolved in 10 mL of sterilized PBS (pH 6.5) and added in 1 mL portions over 1 min to the stirred HSA solution. The mixture was placed in a 37 °C bath and stirred for 20 h, then cooled to room temperature. Solutions of S-PEGylated HSA were transferred to dialysis membrane tubings (MWCO 12.4 kDa for PEG_{5K}-HSA; MWCO 50 kDa for PEG_{20K}-HSA) and gently agitated in 500 mL of deionized water to remove salts and excess mPEG-Mal (2 rounds, > 1 h each). Approximately 90% of each PEG(C34)HSA was set aside for cell culture studies; the remainder was subjected to additional dialysis for characterization. PEG(C34)HSA conjugates could be lyophilized and stored in the dark at 4 °C.

For PEG(C34)HSA conjugates prepared on a multigram scale, purifications were performed with an Amicon stirred ultrafiltration cell (180 mL) equipped with a cellulose membrane filter (100 kDa MWCO), both from Millipore. Reaction mixtures were concentrated to gelatinous slurries (ca. 10 mL), then redispersed in deionized water to maximum volume, and repeated for up to 6 cycles. The rate of filtration ranged from over 10 mL/min to under 1 mL/min, depending on the concentration of residual mPEG-Mal in the retentate.

Protein Characterization. Matrix-assisted laser desorption ionization mass spectra (MALDI-MS) were obtained using an Applied Biosystems Voyager DE PRO spectrometer, equipped with a nitrogen laser (337 nm) and a time-of-flight mass analyzer. Positive-ion MS were obtained in the linear mode using an accelerating voltage of 25 kV, a grid voltage of 94%, and an extraction delay time of 98 ns. The m/z range for this study was 10−100 kDa, using 150 laser shots per spectrum and sinapinic acid as the matrix material.

Circular dichroism (CD) spectra were obtained using a Jasco J-810 spectrophotometer. Protein samples were prepared in halide-free phosphate buffer and diluted to 1 μM. The instrument was flushed with nitrogen for 1 h prior to use; spectra were collected in triplicate from 190−260 nm at a scan rate of 7 min at 25 °C, with data averaging performed after background subtraction. Attenuated total reflectance infrared (ATR-IR) spectra were acquired using a Nicolet Nexus 670 FT-IR, under constant nitrogen flow. Samples were prepared by depositing 1 mL of solution onto the ATR crystal, then dried under a nitrogen stream until a thin film was obtained. The sample chamber was purged for 20 min prior to collecting data.

High-performance liquid chromatography (HPLC) analyses were performed on 100-μL aliquots of PEG(C34)HSA after extensive dialysis, using an Agilent 1100 Series HPLC with a Zorbax XDB-C8 column (Agilent, 4.6 mm × 15 cm). Gradient elutions were performed using 33−66% aqueous CH_3CN with 0.1% trifluoroacetic acid (TFA) at a flow rate of 0.75 mL/min; the column was equilibrated at 33% CH_3CN for at least 30 min prior to sample injection. Proteins were detected by absorbance at 280 nm, with yields determined by peak area integration. Levels of free mPEG-Mal were determined by HPLC at 215 nm, using a Zorbax XDB-C8 column with a gradient elution of 35−45% CH_3CN plus 0.1% TFA (5-kDa mPEG-Mal) or a Phenomenex C18 reversed-phase column (2.0 mm × 5 cm) with a gradient elution of 30−90% CH_3CN plus 0.1% TFA (20-kDa mPEG-Mal), with calibrations against a reference sample. In both cases, the amount of residual Mal-mPEG after six rounds of ultrafiltration was less than 1 wt % (Figure S4, Supporting Information).

Particle Characterization. Nanoparticle tracking analysis (NTA) was performed using a Nanosight LM-10 system equipped with a blue laser (λ = 405 nm), with data analysis supported by NTA v.2.3.5.0033 (Build 16).[50] NTA was performed using PBS (pH 6.5) stored in polyethylene containers. The imaging chamber was cleaned with acetone and a microfiber cloth prior to use, then washed with particle-free water until no background signals were observed. Water was removed from the NTA chamber with a sterile plastic syringe just prior to use and replaced with protein solution (1.0−0.1 mg/mL). Three tracking videos were collected per sample; 50 μL of fresh solution was injected in between each run to prevent protein aggregates from settling, followed by a 60-s recording at a shutter speed of 700 and a gain of 400. The number of tracks per run varied from 300 to 2000, depending on concentration. Hydrodynamic size analysis was derived from the number and volume particle distributions, with population samples based on the number of tracks accumulated over several runs. Optimized parameters for video analysis (advanced mode) include a detection threshold of 10, a 9 × 9 blur setting, and automated settings for track length and minimum particle size.

HSA−PTX Formulation. PTX-HSA formulations were produced from freshly prepared stock solutions of PTX in DMSO (585 μM) and PEG(C34)HSA or n-HSA in PBS adjusted to pH 6.5 (150 μM). PTX solutions were diluted serially with PBS to concentrations at 40× above the target dose. PTX and HSA stock solutions were then combined in a 1:1 v/v ratio (0.4 mL total) and allowed to stand for 4 h at room temperature, prior to use. Then, 10-μL aliquots of HSA−PTX solution were added to 190 μL of cell culture media in 96-well plates containing MCF-7 cells at 10−20% confluence. DMSO concentrations were 0.1% v/v or less; a flowchart describing a protocol for serial dilution is provided in Supporting Information (Figure S1).

Cell Permeation Studies. HUVEC and hCMEC/D3 cells were cultured in T-75 flasks at 37 °C, 5% CO_2, and 90% humidity. HUVECs were cultured in EBM-2 supplemented with Lonza EGM-2 SingleQuots. hCMEC/D3 cells were cultured in EBM-2 supplemented with 5% FBS, 1× penicillin−streptomycin, 1 ng/mL basic fibroblast growth factor, 1.4 μM hydrocortisone, 5 μg/mL ascorbic acid, 1% chemically defined lipid concentrate, and 10 mM HEPES buffer. After thawing, cells were passaged at least three times before transport studies with media changes every other day.

Transport studies were performed in the apical to basolateral direction in triplicate wells simultaneously. HUVECs were seeded between passages 6−10, while hCMEC/D3 cells were seeded at passages 34−42. Cells were seeded onto collagen-coated, 0.4-μm polyester Transwells, at a density of 50,000 cells/cm^2 for HUVECs and 70,000 cells/cm^2 for hCMEC/D3 cells. HUVEC and hCMEC/D3 cells were allowed to proliferate and differentiate for 7 and 14 days, respectively, with exchange of cell culture media every other day. Confluent cell monolayers were washed twice with PBS, then equilibrated for 30 min in HBSS, just prior to permeability studies. Formulations containing [^{14}C]-PTX were added to the apical side of the Transwell plate, which was kept on a rocker tray as aliquots were removed from the donor compartment at 15, 30,

DOI: 10.1021/acs.bioconjchem.5b00143
Bioconjugate Chem. 2015, 26, 941−949

45, 60, and 90 min time points. Initial and remaining donor as well as cell lysate samples were also taken for permeability and mass balance calculations. Then, 100 μL samples were diluted in 4 mL EcoLite scintillation fluid and counted for 5 min on a Beckman Coulter LS 6500 scintillation counter. Apparent permeability (P_{app}) coefficients were determined using the following equation:

$$P_{app} = \frac{dM}{dt} \cdot \frac{1}{SA \times C_0 \times 60}$$

where dM/dt (counts/min) is the steady-state rate of mass transfer, SA (cm^2) is the surface area of the apical membrane, and C_0 (counts) is the initial donor concentration. Studies were compared using an unpaired, two-tailed Student's t-test.

Cell Viability Assays. Mitochondrial oxidation assays using the tetrazolium dye MTT were performed as previously described[51] but using MCF-7 breast cancer cells, which were cultured in T-75 flasks and complete DMEM media with 10% fetal bovine serum (FBS), 1% L-glutamine, and 1% penicillin/streptomycin prior to plating. In a typical experiment, 96-well microtiter plates (5,000 cells/well) were incubated overnight in 200 μL of media to approximately 10% confluence. Solutions in each well were replaced the following day with 190 μL of fresh media and 10 μL of PTX-HSA formulation, followed by 5 days of incubation at 37 °C under a 5% CO_2 atmosphere. The media were removed and replaced with 190 μL fresh media and 10 μL 0.5% MTT, incubated at room temperature for 14 h, then replaced with 200 μL of DMSO for homogenization. Absorbance measurements were recorded on a VersaMax microplate reader at 570 nm with background subtraction; cell viabilities were normalized to a negative control group (having reached 70−90% confluence over 5 days). Experiments were run in triplicate with errors representing one standard deviation; two-tailed probability values were obtained by Student's t test.

■ ASSOCIATED CONTENT

Supporting Information

Flowchart describing PTX-HSA formulations for the in vitro toxicity study; FT-IR spectra; and additional LC analysis of HSA PEGylation. The Supporting Information is available free of charge on the ACS Publications website at DOI: 10.1021/acs.bioconjchem.5b00143.

■ AUTHOR INFORMATION

Corresponding Authors

*(G.K.) E-mail: gknipp@purdue.edu.
*(A.W.) E-mail: alexwei@purdue.edu.

Notes

The authors declare no competing financial interest.

■ ACKNOWLEDGMENTS

This project was supported by the Dane O. Kildsig Center for Pharmaceutical Processing Research and by the Purdue University Center for Cancer Research (P30 CA023168). We thank Tonglei Li (Purdue University) and Pierre-Olivier Couraud (Institut Cochin, Paris, France) for their generous donations of HUVEC and hCMEC/D3 cells, respectively.

■ REFERENCES

(1) Kosaka, N., Ogawa, M., Choyke, P. L., Karassina, N., Corona, C., McDougall, M., Lynch, D. T., Hoyt, C. C., Levenson, R. M., V. Los, G. V., et al. (2009) *In vivo* Stable Tumor-Specific Painting in Various Colors Using Dehalogenase Based Protein-Tag Fluorescent Ligands. *Bioconjugate Chem. 20*, 1367−1374.

(2) Atkinson, S. F., Bettinger, T., Seymour, L. W., Behr, J. P., and Ward, C. M. (2001) Conjugation of Folate via Gelonin Carbohydrate Residues Retains Ribosomal-Inactivating Properties of the Toxin and Permits Targeting to Folate Receptor Positive Cells. *J. Biol. Chem. 276*, 27930−27935.

(3) Sinclair, A. M., and Elliot, S. (2005) Glycoengineering: The Effect of Glycosylation on the Properties of Therapeutic Proteins. *J. Pharm. Sci. 94*, 1626−1635.

(4) Molino, N. M., Bilotkach, K., Fraser, D. A., Ren, D., and Wang, S. W. (2012) Complement Activation and Cell Uptake Responses toward Polymer-Functionalized Protein Nanocapsules. *Biomacromolecules 13*, 974−981.

(5) Monfardini, C., and Veronese, M. F. (1998) Stabilization of Substances in Circulation. *Bioconjugate Chem. 9*, 418−450.

(6) López-Alonso, J. P., Diez-García, F., Font, J., Ribó, M., Vilanova, M., Scholtz, J. M., González, C., Vottariello, F., Gotte, G., Libonati, M., et al. (2009) Carbodiimide EDC Induces Cross-Links That Stabilize RNase A C-Dimer against Dissociation: EDC Adducts Can Affect Protein Net Charge, Conformation, and Activity. *Bioconjugate Chem. 20*, 1459−1473.

(7) Chalker, J. M., Bernardes, G. J. L., Lin, Y. A., and Davis, B. G. (2009) Chemical Modification of Proteins at Cysteine: Opportunities in Chemistry and Biology. *Chem.—Asian J. 4*, 630−640.

(8) Broersen, K., Weijers, M., de Groot, J., Hamer, R. J., and de Jongh, H. H. J. (2007) Effect of Protein Charge on the Generation of Aggregation-Prone Conformers. *Biomacromolecules 8*, 1648−1656.

(9) Gao, J. P., Yong, Z. H., Zhang, F., Ruan, K. C., Xu, C. H., and Chen, G. Y. (2005) Positive Charges on Lysine Residues of the Extrinsic 18 kDa Protein Are Important to Its Electrostatic Interaction with Spinach Photosystem II Membranes. *Acta Biochim. Biophys. Sin. 37*, 737−742.

(10) Harris, J. M., and Chess, R. B. (2003) Effect of Pegylation on Pharmaceuticals. *Nat. Rev. Drug Discovery 2*, 214−221.

(11) Ryan, S. M., Mantovani, G., Wang, X., Haddleton, D. M., and Brayden, D. J. (2008) Advances in PEGylation of Important Biotech Molecules: Delivery Aspects. *Expert Opin. Drug Delivery 5*, 371−383.

(12) Duncan, R., and Gaspar, R. (2011) Nanomedicine(s) under the Microscope. *Mol. Pharmaceutics 8*, 2101−2141.

(13) Nischan, N., and Hackenberger, C. P. R. (2014) Site-Specific PEGylation of Proteins– Recent Developments. *J. Org. Chem. 79*, 10727−10733.

(14) Meng, W., Guo, X., Qin, M., Pan, H., Cao, Y., and Wang, W. (2012) Mechanistic Insights into the Stabilization of srcSH3 by PEGylation. *Langmuir 28*, 16133−16140.

(15) Rodríguez-Martínez, J. A., Solá, R. J., Castillo, B., Cintrón-Colón, H. R., Rivera-Rivera, I., Barletta, G., and Griebenow, K. (2008) Stabilization of *a*-Chymotrypsin upon PEGylation Correlates with Reduced Structural Dynamics. *Biotechnol. Bioeng. 101*, 1142−1149.

(16) Ghuman, J., Zunszain, P. A., Petitpas, I., Bhattacharya, A. A., Otagiri, M., and Curry, S. (2005) Structural Basis of the Drug-Binding Specificity of Human Serum Albumin. *J. Mol. Biol. 353*, 38−52.

(17) Paál, K., Müller, J., and Hegedûs, L. (2001) High Affinity Binding of Paclitaxel to Human Serum Albumin. *Eur. J. Biochem. 8*, 2187−2191.

(18) John, T. A., Vogel, S. M., Tiruppathi, C., Malik, A. B., and Minshall, R. D. (2003) Quantitative Analysis of Albumin Uptake and Transport in the Rat Microvessel Endothelial Monolayer. *Am. J. Physiol. Lung Cell. Mol. Physiol. 284*, 187−196.

(19) Schubert, W., Frank, P. G., Razani, B., Park, D. S., Chow, C. W., and Lisanti, M. P. (2001) Caveolae-Deficient Endothelial Cells Show Defects in the Uptake and Transport of Albumin *in Vivo*. *J. Biol. Chem. 276*, 48619−48622.

(20) Peters, T. (1996) *All about Albumin: Biochemistry, Genetics, and Medical Applications*, Academic Press, San Diego, CA.

DOI: 10.1021/acs.bioconjchem.5b00143
Bioconjugate Chem. 2015, 26, 941−949

(21) Kratz, F. (2008) Albumin as a Drug Carrier: Design of Prodrugs, Drug Conjugates and Nanoparticles. *J. Controlled Release 132*, 171−183.
(22) Elsadek, B., and Kratz, F. (2012) Impact of Albumin on Drug Delivery — New Applications on the Horizon. *J. Controlled Release 157*, 4−28.
(23) Desai, N. *Nab* Technology: A Drug Delivery Platform Utilizing Endothelial gp60 Receptor-Based Transport and Tumour-Derived SPARC for Targeting, in *Drug Delivery Report*, 16th ed., PharmaVentures, Ltd.: Oxford; Winter 2007/2008, pp 37−41.
(24) Desai, N. V., Trieu, Z., Yao, Z., Louie, L., Ci, S., Yang, A., Tao, C., De, T., Beals, B., Dykes, D., et al. (2006) Increased Antitumor Activity, Intratumor Paclitaxel Concentrations, and Endothelial Cell Transport of Cremophor-Free, Albumin-Bound Paclitaxel, ABI-007, Compared with Cremophor-Based Paclitaxel. *Clin. Cancer Res. 12*, 1317−1324.
(25) Green, M. R., Manikhas, G. M., Orlov, S., Afanasyev, B., Makhson, A. M., Bhar, P., and Hawkins, M. J. (2006) Abraxane®, a Novel Cremophor®-Free, Albumin-Bound Particle Form of Paclitaxel for the Treatment of Advanced Non-small-cell Lung Cancer. *Ann. Oncol. 17*, 1263−1268.
(26) Von Hoff, D. D., Ervin, T., Arena, F. P., Chiorean, E. G., Infante, J., Moore, M., Seay, T., Tjulandin, S. A., Ma, W. W., Saleh, M. N., et al. (2013) Increased Survival in Pancreatic Cancer with nab-Paclitaxel Plus Gemcitabine. *New Engl. J. Med. 369*, 1691−1703.
(27) Kavallaris, M. (2010) Microtubules and Resistance to Tubulin-Binding Agents. *Nat. Rev. Cancer 10*, 194−204.
(28) Gelderblom, H., Verweij, J., Nooter, K., and Sparreboom, A. (2001) Cremophor EL: The Drawbacks and Advantages of Vehicle Selection for Drug Formulation. *Eur. J. Cancer 37*, 1590−1598.
(29) Anil, K. S., Alka, G., and Aggarwal, D. (2002) Paclitaxel and Its Formulations. *Int. J. Pharm. 235*, 179−192.
(30) Marupudi, N. I., Han, J. E., Li, K. W., Renard, V. M., Tyler, B. M., and Brem, H. (2007) Paclitaxel: A Review of Adverse Toxicities and Novel Delivery Strategies. *Expert. Opin. Drug Saf. 5*, 609−621.
(31) Aigner, J., Marme, F., Smetanay, K., Schuetz, F., Jaeger, D., and Schneeweiss, A. (2013) Nab-Paclitaxel Monotherapy as a Treatment of Patients with Metastatic Breast Cancer in Routine Clinical Practice. *Anticancer Res. 33*, 3407−3413.
(32) Ko, Y. J., Canil, C. M., Mukherjee, S. D., Winquist, E., Elser, C., Eisen, A., Reaume, M. N., Zhang, L. Y., and Sridhar, S. S. (2013) Nanoparticle Albumin-Bound Paclitaxel for Second-Line Treatment of Metastatic Urothelial Carcinoma: A Single Group, Multicentre, Phase 2 Study. *Lancet Oncol. 14*, 769−776.
(33) Dosio, F., Arpicco, S., and Brusa, P. (2001) Poly(ethylene glycol) Human Serum Albumin−Paclitaxel Conjugates: Preparation, Characterization and Pharmacokinetics. *J. Controlled Release 76*, 107−117.
(34) Meng, F., Manjula, B. N., Smith, P. K., and Acharya, S. A. (2008) PEGylation of Human Serum Albumin: Reaction of PEG-Phenyl-Isothiocyanate with Protein. *Bioconjugate Chem. 19*, 1352−1360.
(35) Plesner, B., Fee, C. J., Westh, P., and Nielsen, A. D. (2011) Effects of PEG Size on Structure, Function and Stability of PEGylated BSA. *Eur. J. Pharm. Biopharm. 7*, 399−405.
(36) Zhao, T., Cheng, Y. N., Tan, H. N., Liu, J. F., Xu, H. L., Pang, G. L., and Wang, F. S. (2012) Site-Specific Chemical Modification of Human Serum Albumin with Polyethylene Glycol Prolongs Half-Life and Improves Intravascular Retention in Mice. *Biol. Pharm. Bull. 35*, 280−288.
(37) Schumacher, F. F., Nobles, M., Ryan, C. P., Smith, M. E. B., Tinker, A., Caddick, S., and Baker, J. R. (2011) In Situ Maleimide Bridging of Disulfides and a New Approach to Protein PEGylation. *Bioconjugate Chem. 22*, 132−136.
(38) Smith, M. E. B., Schumacher, F. F., Ryan, C. P., Tedaldi, L. M., Papaioannou, D., Waksman, G., Caddick, S., and Baker, J. R. (2010) Protein Modification, Bioconjugation, and Disulfide Bridging Using Bromomaleimides. *J. Am. Chem. Soc. 132*, 1960−1965.
(39) (a) Katchalski, E., Benjamin, G. S., and Gross, V. (1957) The Availability of the Disulfide Bonds of Human and Bovine Serum Albumin and of Bovine γ-Globulin to Reduction by Thioglycolic Acid. *J. Am. Chem. Soc. 79*, 4096−4099. (b) Yang, M., Dutta, C., and Tiwari, A. (2015) Disulfide-Bond Scrambling Promotes Amorphous Aggregates in Lysozyme and Bovine Serum Albumin. *J. Phys. Chem. B 119*, 3969−3981.
(40) Kobayashi, K., Nakamura, N., Sumi, A., Ohmura, T., and Yokoyama, K. (1998) The Development of Recombinant Human Serum Albumin. *Ther. Apheresis 2*, 257−262.
(41) MALDI-MS peaks at *m/z* 33,372 and 22,326 could also be observed, corresponding to doubly and triply protonated species, respectively.
(42) Kim, Y., Ho, S. O., Gassman, N. R., Korlann, Y., Landorf, E. V., Collart, F. R., and Weiss, S. (2008) Efficient Site-Specific Labeling of Proteins via Cysteines. *Bioconjugate Chem. 19*, 786−791.
(43) It is worth noting that the cytotoxicity of PTX in the absence of HSA may be influenced by the amount of residual DMSO. In this study, PTX solutions were prepared by serial dilution with PBS and/or HSA in PBS from a 585 μM stock solution in DMSO (see Figure S1, Supporting Information).
(44) PTX at the same concentration in PBS without HSA also formed large (>200 nm) aggregates over the same period of time.
(45) Weksler, B., Romero, I. A., and Couraud, P. O. (2013) The hCMEC/D3 Cell Line as a Model of the Human Blood Brain Barrier. *Fluids Barriers CNS 10*, 16.
(46) Otani, M., Natsume, T., Watanabe, J. I., Kobayashi, M., Murakoshi, M., Mikami, T., and Nakayama, T. (2000) TZT-1027, an Antimicrotubule Agent, Attacks Tumor Vasculature and Induces Tumor Cell Death. *Jpn. J. Cancer Res. 91*, 837−844.
(47) Higher PTX concentrations were necessary, due to the limited efficiency of PTX radiolabeling and sensitivity of the scintillation detector. PTX concentrations in the basolateral compartment are estimated to be 0.1−10 nM, depending on the time point.
(48) Jang, S. H., Wientjes, M. G., and Au, J. L. (2001) Kinetics of P-Glycoprotein-Mediated Efflux of Paclitaxel. *J. Pharmacol. Exp. Ther. 298*, 1236−1242.
(49) Surapaneni, M. S., Das, S. K., and Das, N. G. (2012) Designing Paclitaxel Drug Delivery Systems Aimed at Improved Patient Outcomes: Current Status and Challenges. *ISRN Pharmacol. 2012*, 623139.
(50) Later versions of this software have been tested and found to produce very similar results.
(51) Mehtala, J. G., Torregrosa-Allen, S., Elzey, B. D., Jeon, M., Kim, C., and Wei, A. (2014) Synergistic Effects of Cisplatin Chemotherapy and Gold Nanorod-Mediated Hyperthermia on Ovarian Cancer Cells. *Nanomedicine 9*, 1939−1955.

DOI: 10.1021/acs.bioconjchem.5b00143
Bioconjugate Chem. 2015, 26, 941−949